The Effects of Displacement Induced by Thermal Perturbations on the Structure and Stability of Boundary-Layer Flows[1]

C. Treviño

A. Liñán

Abstract. The free-interaction influence of a thermal expansion process in boundary-layer gas flow is analyzed using the formalism of triple-deck theory. The physical model considered is the forced convection of a gas flowing over a flat plate subject to a heated slab. Both linearized and full nonlinear solutions are obtained using Fourier transform methods and spectral numerical techniques. The influence of monochromatic thermal perturbation on boundary-layer stability (lower branch) is studied and first-order correction of the lower branch neutral stability curve for the boundary-layer flow has been obtained. The shift of neutral stability is then computed for different values of the thermal perturbation wave number, making unstable some otherwise stable modes.

1. Introduction

In a gaseous boundary-layer flow the expansion and displacement effects due to surface thermal distrubances can be very important and therefore can modify the flow structure and stability. In particular, if the surface temperature changes abruptly in a small region, the velocity and pressure gradients generated can be very strong and the effects have to be retained to leading order in boundary-layer analysis. These pressure gradients are generated by interaction with the outer potential flow and have an important influence on the fluid close to the wall where the convective terms are small. The triple-deck structure can be used to explain these types of flows correctly and to predict boundary-layer separation. Gas expansion due to heating or cooling is produced in a viscous nonisothermal lower deck and is impressed as displacement effects, thus generating pressure gradients, in the upper deck. The triple-deck concept has been introduced in the classical works by Stewartson and Williams [1], Messiter [2], and Stewartson [3] studying the influence on the drag coefficient of a finite-length flat plate, using a three-layer structure. A comprehensive review on this subject is given by Smith [4], where the same structural argument of triple-deck theory can be applied immediately to many other incompressible and compressible problems. The effects of surface temperature changes in a vertical flat plate on the free convective flow structure were analyzed by Messiter

and Liñán [5]. Due to the lack of an upper-deck flow, the analysis can be carried out by a two-layer concept, where the resulting equations for the lower viscous and heat-conducting sublayer, are linear. However, when describing the effect of surface change in temperature on a forced boundary-layer flow, triple-deck analysis is then required. Recently, Méndez *et al.* [6] studied the fluid mechanical structure of a gaseous forced boundary-layer flow produced by the thermal expansion process using triple-deck theory. They analyzed the case of a step-change on surface temperature. The effects of the displacement, due to gas expansion resulting from the sudden temperature rise, increase strongly when increasing the temperature ratio, defined by the ratio of the maximum plate temperature to the fluid temperature. For a critical value of this parameter, flow separation, ahead of the point where the surface temperature changes, can be reached. This critical value is close to $3Pr^{1/3}$ for a perfect gas. Pr is the Prandtl number which relates viscous with thermal diffusivity. Fluids with a large Prandtl number make the expansion process weaker and thus a larger temperature ratio is needed to obtain flow separation. The effects of thermal expansion are felt in a region, around the point where the temperature changes, of size (related to the boundary-layer thickness h^*) of the order of $R_h^{1/4}$, where R_h is the Reynolds number based on the boundary-layer thickness.

The changes in the flow structure due to thermal perturbations have a strong influence on the stability of the boundary-layer flow. In relation to flow stability, the triple-deck structure is appropriate in the lower branch of the neutral stability curve for large Reynolds numbers. In this limit, therefore, full interaction with the outer potential flow must be considered [7]. Linear and weakly nonlinear stability analyses were carried out by Smith [7] [9], where nonparallel effects were also included. He obtained a dispersion relation in terms of the Airy function and solved it numerically. Goldstein [10] and Goldstein and Hultgren [11] developed an analysis to study the coupling between a small but sudden variation in surface geometry and small amplitude acoustic waves. The objective was to explain the receptivity measurements carried out by Leehey and Shapiro [12], who obtained a high value of the coupling coefficient. Bodonyi *et al.* [13] numerically studied this receptivity problem but with finite size surface variations.

Surface cooling effects on compressible boundary-layer flows have been addressed by several works [14]–[16]. Seddougui *et al.* [14] studied the influence of wall cooling on boundary-layer instability. They found that moderate surface cooling can enhance the Tollmien–Schlichting viscous mode activity, where the spatial growth of viscous modes can be comparable with inviscid ones. They also found that cooling can destabilize otherwise stable viscous and inviscid modes at any Mach number. They obtained good agreement with the experimental results of Lysenko and Maslov [15]. On the other hand, strong wall cooling in a hypersonic flow has been analyzed by Brown *et al.* [16]. They concluded, from the numerical solutions of the triple-deck in the weak global interaction regime, that separation and reattachment on a compressive ramp cannot be effectively eliminated or delayed by lowering the wall temperature, but as the wall temperature is reduced the triple-deck dimension decreases drastically and, therefore, the upstream influence. In all the works a uniform wall temperature was assumed.

There are many interesting low Mach number flows with strong temperature gradients which can be analyzed using the framework of the triple-deck concept. There is experimental evidence that premixed flames are stabilized by aerodynamic effects such as low local velocities and even flow recirculation that would not exist without the presence of the flame. These recirculating flows are generated by pressure gradients that are induced by the interaction of the flame with the inviscid flow producing the separation of the boundary layer [17]. In diffusion flame experiments in boundary layers with injection, pressure gradients have been predicted from the measured velocity field in the vicinity of the flame leading edge [18]. The existence of low- and high-pressure regions suggests the possibility of using higher-order effects in the boundary-layer approximation that influences the structure and showing the interactions between the flame and flow field. In particular, higher-order effects are very important in processes with density variations. In this case the expansion of the gas flowing along the body changes in an important way the displacement thickness, producing a strong interaction with the potential flow. Higher-order effects in combustion processes were considered in several works [19], [20]. There is also interest in the study of reacting flows over catalytic surfaces. In this case the surface temperature can increase in a short distance depending on the sizes of the active sites on the catalytic wall.

In this work we use spectral numerical techniques to describe the strong surface thermal perturbation in a region assumed to be of size of the order of the triple-deck. Therefore, the problem can be scaled using the classical triple-deck scaling laws, as shown for the case of a step change in surface temperature [6]. In the analysis we treat in detail the case (for simplicity) when the surface temperature is equal to the ambient

temperature, except in the triple-deck region of the order of $R_h^{1/4}$ times the boundary-layer thickness, where the temperature can assume any arbitrary form. Also for simplicity we assume an ideal gas with a unity Chapman–Rubesin parameter (viscosity coefficient linearly dependent on tempeature). The changes in pressure induced by gas expansion and felt on the upper deck as displacement effects, are assumed to be very strong in comparison with that of the free stream in the unperturbed flow. If we increase the temperature, an overpressure zone appears in the upstream region followed by an underpressure zone downstream. Therefore, there are two zones with adverse pressure gradients and thus two regions where the shear stresses at the wall (skin friction) are lower than the initial values. The region in between presents a strong peak in positive skin friction. On the other hand, if the temperature in the triple-deck region is smaller than the ambient one (cooling), the effects are reversed with a single region with adverse pressure gradients resulting in a strong reduction in minimum skin friction. In Section 2 we present the nondimensional triple-deck governing equations, retaining the unsteady terms for use in the stability analysis, assuming that the characteristic time of change is of the order of the residence time in the triple-deck region. In Section 3 we present the analysis of the linearized response of the boundary layer under small perturbations in the surface temperature, obtaining the results by using Fourier transform techniques. Nonlinear analysis is given in Section 4, using numerical methods based on spectral techniques. We assume here the case for a smooth surface-temperature distribution. A stability analysis is presented in Section 5 by assuming a monochromatic surface-temperature perturbation. We are interested in the shift of the neutral stability curve when surface thermal perturbations are present in a gaseous boundary-layer flow. Finally, concluding remarks are presented in Section 6.

2. Governing Equations

The physical model analyzed is the following. We consider a gaseous boundary-layer flow past a body of arbitrary shape, as shown in Figure 1. The wall temperature is assumed for simplicity to be the same as the free-stream temperature, T_∞^*, except in a small region of order $h^* R_h^{1/4}$ around a point $(x^* = x_0^*, y^* = 0)$, where the boundary-layer thickness is h^* and the free-stream velocity is v_e^*. Here, R_h denotes the Reynolds number based on the boundary-layer thickness, $R_h = (\rho_\infty^* v_e^* h^*)/\mu_\infty^*$. ρ_∞^* and μ_∞^* represent the gas density and the viscosity coefficient in the free stream, respectively. Assuming the heated/cooled region to be confined in a streamwise length of order $h^* R_h^{1/4}$, the free interaction phenomena can be described by the triple-deck flow structure. The wall-temperature difference in this region, $T_w^* - T_\infty^*$, can take any arbitrary form, tending to zero at both ends of the heated/cooled triple-deck region. The evolution of the displacement thickness changes in an important way due to the expansion $(T_w^* > T_\infty^*)$ or compression $(T_w^* < T_\infty^*)$ process, causing retention of the pressure gradients in the leading-order governing equations. The triple-deck structure can be described by three layers (upper, main, and lower deck), each satisfying appropriated governing equations [4]. For this problem, the viscous and nonisothermal effects are concentrated in the lower deck,

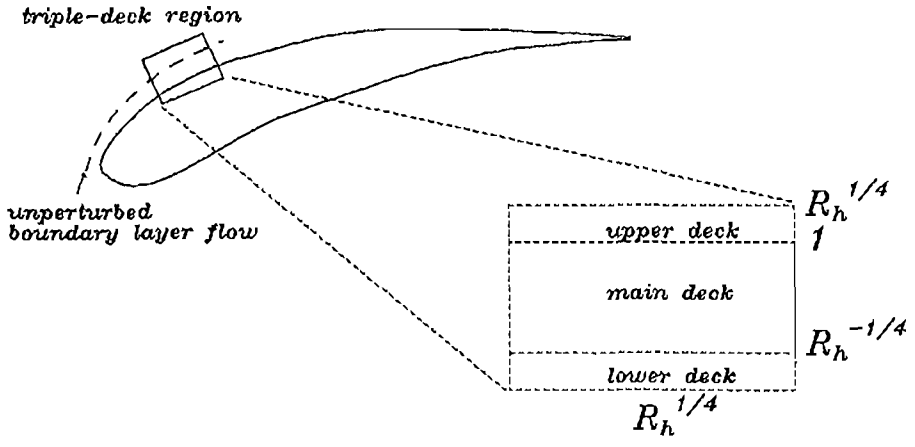

Figure 1. Schematical diagram of the interaction problem.

while the flow in the main and upper decks is incompressible and inviscid. The gas expansion generated in the lower deck produces, after being transmitted through the main deck, displacement effects in the upper deck. The governing equations in the isothermal upper deck reduce to the well-known pressure-displacement relation [3], to be given later. The main deck transmits the pressure gradients down to the lower deck. In order to consider those regions where the thermal expansion/compression becomes considerable, it is necessary to introduce adequate triple-deck structure scaling. The nondimensional unsteady governing equations in the lower deck, assuming the Eckert number to be completely negligible (low Mach number flows), are given by

$$\frac{\partial \rho}{\partial \tilde{t}} + \frac{\partial(\rho \tilde{u})}{\partial \tilde{x}} + \frac{\partial(\rho \tilde{v})}{\partial \tilde{y}} = 0, \tag{1}$$

$$\rho \frac{\partial \tilde{u}}{\partial \tilde{t}} + \rho \tilde{u} \frac{\partial \tilde{u}}{\partial \tilde{x}} + \rho \tilde{v} \frac{\partial \tilde{v}}{\partial \tilde{y}} = -\frac{\partial \tilde{p}}{\partial \tilde{x}} + \frac{\partial}{\partial \tilde{y}}\left(\mu \frac{\partial \tilde{u}}{\partial \tilde{y}}\right), \tag{2}$$

$$\frac{\partial p}{\partial y} = O(R_h^{-1}), \tag{3}$$

$$\rho \frac{\partial T}{\partial \tilde{t}} + \rho \tilde{u} \frac{\partial T}{\partial \tilde{x}} + \rho \tilde{v} \frac{\partial T}{\partial \tilde{y}} = \frac{1}{Pr} \frac{\partial}{\partial \tilde{y}}\left(\mu \frac{\partial T}{\partial \tilde{y}}\right), \tag{4}$$

where the nondimensional variables are defined by

$$\tilde{x} = \frac{(x^* - x_0^*)}{h^* R_h^{1/4}}, \qquad \tilde{y} = \frac{y^* R_h^{1/4}}{h^*}, \qquad \tilde{u} = \frac{u^* R_h^{1/4}}{v_e^*}, \qquad \tilde{v} = \frac{v^* R_h^{3/4}}{v_e^*},$$

$$\tilde{p} = \frac{(p^* - p_e^*) R_h^{1/2}}{\rho_\infty^* v_e^{*2}}, \qquad \tilde{t} = \frac{v_e^* t^*}{h^* R_h^{1/2}}, \qquad \mu = \frac{\mu^*}{\mu_\infty^*}, \qquad \rho = \frac{\rho^*}{\rho_\infty^*}, \qquad T = \frac{T^*}{T_\infty^*}. \tag{5}$$

In the above equations x^* and y^* correspond to the longitudinal and normal coordinates, respectively; u^* and v^* correspond to the fluid velocity components in the x^* and y^* directions, respectively; p^* is the pressure and p_e^* is the pressure of the unperturbed flow at the position $x^* = x_0^*$; t^* is the time. The boundary-layer thickness h^* is defined in such a way that it makes the velocity gradient at the wall of the unperturbed flow equal to v_e^*/h^*; Pr represents the Prandtl number defined by $Pr = \mu_\infty^* C_p^*/k_\infty^*$, where C_p^* is the specific heat at constant pressure and k_∞^* represents the heat conductivity coefficient of the gas. We also assume that the Prandtl number is constant. In addition to the above equations, we need an equation of state. In this case, for simplicity, we use an ideal gas law given by $p^* = p_e^* \rho T$, with a gas viscosity coefficient linearly dependent on temperature (Chapman–Rubesin parameter, $C = \mu\rho = 1$). For low Mach number flows, the pressure variations are small compared with the ambient pressure and therefore the pressure can be assumed to be constant only for the state equation. It can be written in nondimensional form as

$$\rho T = 1. \tag{6}$$

The boundary conditions required to complete the problem statement are specified by the following relationships: at $\tilde{y} = 0$,

$$\tilde{u} = \tilde{v} = 0, \qquad T = T_w(\tilde{x}), \qquad \text{with} \quad T \to 1 \quad \text{for} \quad |\tilde{x}| \to \infty. \tag{7}$$

As $|\tilde{x}| \to \infty$, the solution must match the unperturbed flow solution given by $\tilde{u} \to \tilde{y}$ and $T \to 1$. For large values of $\tilde{y}$, the solution must match that of the main deck. We do not go into details that can be found elsewhere [3]. The corresponding boundary conditions for large $\tilde{y}$ are then given by

$$\tilde{u} \sim \tilde{y} + \tilde{A}(\tilde{x}, \tilde{t}) \qquad \text{for} \quad \tilde{y} \to \infty. \tag{8}$$

Here $-\tilde{A}(\tilde{x}, \tilde{t})$ represents the displacement thickness and also the velocity slip at the base of the main deck, corresponding to the inviscid perturbation of the upstream solution by the induced pressure gradient. In addition, a boundary condition for the temperature is required in order to complete the match with the main-deck solution and is given by

$$T \to 1 \qquad \text{for} \quad \tilde{y} \to \infty. \tag{9}$$

Finally, an interaction condition, which is derived by thin airfoil linearized theory, is required to match the upper-deck solution and it corresponds to the well-known pressure-displacement relation [3]

$$\tilde{p}(\tilde{x},\tilde{t})=\frac{1}{\pi}\int_{-\infty}^{\infty}\frac{\partial\tilde{A}(\tilde{x}_1,\tilde{t})}{\partial\tilde{x}_1}\frac{d\tilde{x}_1}{(\tilde{x}-\tilde{x}_1)}. \tag{10}$$

In the last equation, the integral represents the principal value of the Cauchy–Hilbert integral. Clearly, for fixed values of R_h and Pr, the solution depends on the magnitude and distribution of $T_w(\tilde{x})$. The above set of equations defines the thermal expansion/compression problem within the longitudinal scale $(x^*-x_0^*)\sim h^*R_h^{1/4}$. However, for the Pr and $\mu\rho$ constants, these equations can be simplified even more by employing the Howarth–Dorodnitzyn transformation [21], giving an equivalent set of quasi-incompressible governing equations. By introducing the following nondimensional variables,

$$\bar{x}=\tilde{x},\qquad \bar{y}=\int_0^{\tilde{y}}\frac{d\tilde{y}}{T},\qquad \bar{t}=\tilde{t},\qquad \bar{u}=\tilde{u},\qquad \bar{v}=\frac{\tilde{v}}{T}+\tilde{u}\frac{\partial\bar{y}}{\partial\tilde{x}}+\frac{\partial\bar{y}}{\partial\tilde{t}}, \tag{11}$$

we obtain the corresponding lower-deck nondimensional governing equations:

$$\frac{\partial\bar{u}}{\partial\bar{x}}+\frac{\partial\bar{v}}{\partial\bar{y}}=0, \tag{12}$$

$$\frac{\partial\bar{u}}{\partial\bar{t}}+\bar{u}\frac{\partial\bar{u}}{\partial\bar{x}}+\bar{v}\frac{\partial\bar{u}}{\partial\bar{y}}=-T\frac{d\tilde{p}}{d\bar{x}}+\frac{\partial^2\bar{u}}{\partial\bar{y}^2}, \tag{13}$$

$$\frac{\partial T}{\partial\bar{t}}+\bar{u}\frac{\partial T}{\partial\bar{x}}+\bar{v}\frac{\partial T}{\partial\bar{y}}=\frac{1}{Pr}\frac{\partial^2 T}{\partial\bar{y}^2}. \tag{14}$$

Equations (12)–(14) have to be solved with the following boundary conditions,

$$\begin{aligned}&\bar{u}=\bar{v}=0,\quad T=T_w(\bar{x})\qquad \text{at}\quad \bar{y}=0,\\ &\bar{u}\to\bar{y},\qquad T\to 1\qquad \text{for}\quad |\bar{x}|\to\infty,\\ &\bar{u}\to\bar{y}+\tilde{A}(\bar{x},\bar{t})+\int_0^{\infty}(T-1)\,d\bar{y}\qquad \text{for}\quad y\to\infty,\end{aligned} \tag{15}$$

and the appropriate initial conditions. The nonconstant nondimensional density, $\rho=1/T$, does not fully disappear from the governing equations, but remains only in the pressure-gradient term in the momentum equation (13). The lower-deck equations are completed with the interaction relationship

$$\tilde{p}(\bar{x},\bar{t})=\frac{1}{\pi}\int_{-\infty}^{\infty}\frac{\partial\tilde{A}(\bar{x}_1,\bar{t})}{\partial\bar{x}_1}\frac{d\bar{x}_1}{(\bar{x}-\bar{x}_1)}. \tag{16}$$

Using the new lower-deck normal coordinate $\bar{y}$ allows us to separate the displacement effects denoted by $\tilde{A}(\bar{x}_1,\bar{t})$ and the gas-expansion effects denoted by the integral term $\int_0^{\infty}(T-1)\,d\bar{y}$. In the next two sections we analyze both the linear and nonlinear steady flows induced by a heated/cooled slab.

3. Linearized Theory For $T_w\to 1$

Equations (12)–(16) can be solved analytically by assuming that the surface-temperature changes are very small compared with the ambient temperature. Defining a small parameter δ as the maximum nondimensional temperature difference, $\delta=\max(T_w-1)$, the lower-deck governing equations can be linearized around the undisturbed boundary-layer profile, by expanding the flow variables as follows:

$$\begin{aligned}u=\bar{y}+\hat{u}=\bar{y}+\delta\hat{u}_0+\cdots,\qquad \bar{v}=\delta\hat{v}_0+\cdots,\\ \tilde{p}=\delta\hat{p}_0+\cdots,\qquad \tilde{A}=\delta\hat{A}_0+\cdots,\\ T=1+\hat{T}=1+\delta\hat{T}_0+\cdots,\qquad \tau=1+\hat{\tau}=1+\delta\hat{\tau}_0+\cdots,\end{aligned} \tag{17}$$

where τ corresponds to the nondimensional skin friction defined by $\tau=d\bar{u}/d\bar{y}$, which is exactly unity for the unperturbed isothermal boundary-layer flow. Therefore, the linear nondimensional governing equations

can be reduced, up to first order, to

$$\frac{\partial \hat{u}_0}{\partial \bar{x}} + \frac{\partial \hat{v}_0}{\partial \bar{y}} = 0,$$

$$\bar{y}\frac{\partial \hat{\tau}_0}{\partial \bar{x}} - \frac{\partial^2 \hat{\tau}_0}{\partial \bar{y}^2} = 0, \tag{18}$$

$$\bar{y}\frac{\partial \hat{T}_0}{\partial \bar{x}} - \frac{1}{Pr}\frac{\partial^2 \hat{T}_0}{\partial \bar{y}^2} = 0,$$

and

$$\frac{\partial \hat{u}_1}{\partial \bar{x}} + \frac{\partial \hat{v}_1}{\partial \bar{y}} = 0,$$

$$\bar{y}\frac{\partial \hat{\tau}_1}{\partial \bar{x}} - \frac{\partial^2 \hat{\tau}_1}{\partial \bar{y}^2} = -\hat{u}_0\frac{\partial \hat{\tau}_0}{\partial \bar{x}} - \hat{v}_0\frac{\partial \hat{\tau}_0}{\partial \bar{y}} - \frac{d\hat{p}_0}{d\bar{x}}\frac{\partial \hat{T}_0}{\partial \bar{y}}, \tag{19}$$

$$\bar{y}\frac{\partial \hat{T}_1}{\partial \bar{x}} - \frac{1}{Pr}\frac{\partial^2 \hat{T}_1}{\partial \bar{y}^2} = -\hat{u}_0\frac{\partial \hat{T}_0}{\partial \bar{x}} - \hat{v}_0\frac{\partial \hat{T}_0}{\partial \bar{y}},$$

etc., with the following boundary conditions:

$$\hat{u}_n = \hat{v}_n = 0, \quad \hat{T}_0 = \hat{T}_w(\bar{x}), \quad \hat{T}_n = 0 (n \neq 0), \quad \frac{\partial \hat{\tau}_n}{\partial \bar{y}} = (1 + \hat{T}_{n-1})\frac{d\hat{p}_n}{d\bar{x}} \qquad \text{at} \quad \bar{y} = 0,$$

$$\hat{u}_n \to 0, \quad \hat{T}_n \to 0 \qquad \text{for} \quad |\bar{x}| \to \infty,$$

$$\hat{u}_n \to \hat{A}_n + \int_0^\infty \hat{T}_n(\bar{x}, \bar{y})\, d\bar{y}, \quad \hat{T}_n \to 0 \qquad \text{for} \quad \bar{y} \to \infty,$$

and

$$\hat{p}_n(\bar{x}) = \frac{1}{\pi}\int_{-\infty}^{\infty} \frac{d\hat{A}_n(\bar{x}_1)}{d\bar{x}_1}\frac{d\bar{x}_1}{(\bar{x} - \bar{x}_1)}.$$

The leading-order solution can be obtained using the Fourier transform defined for all variables as, for example,

$$\tau_{0F}(\bar{y}) = \int_{-\infty}^{\infty} \hat{\tau}(\bar{x}, \bar{y}) \exp(-ik\bar{x})\, d\bar{x}. \tag{20}$$

The transformed equations are then given by

$$ik\bar{y}\tau_{0F} = \frac{d^2\tau_{0F}}{d\bar{y}^2}, \tag{21}$$

$$ik\bar{y}\, Pr\, T_{0F} = \frac{d^2 T_{0F}}{d\bar{y}^2}, \tag{22}$$

with the following boundary conditions:

$$T_{0F}(0) = T_{wF}, \qquad \left.\frac{d\tau_{0F}}{d\bar{y}}\right|_{y=0} = ik|k|\int_0^\infty (\tau_{0F} - T_{0F})\, d\bar{y},$$

$$\tau_{0F}(\infty) \to 0, \qquad T_{0F}(\infty) \to 0,$$

for any value of the wave number k. The first step is to obtain the solution up to the order of δ. In this case the energy equation decouples from the continuity and momentum equations. The solution to (22) is

$$T_{0F} = T_{wF}\frac{Ai[(ik\, Pr)^{1/3}\bar{y}]}{Ai[0]}, \tag{23}$$

where Ai represents the Airy function. The solution to (21) with the appropriate boundary conditions is

$$\tau_{0F} = \frac{T_{wF} ik|k| Ai[(ik)^{1/3}\bar{y}]}{Pr^{1/3} Ai[0](ik|k| - (ik)^{2/3} Ai'[0])}. \tag{24}$$

The pressure in Fourier space is given by

$$p_{0F} = \frac{T_{wF}|k|(ik)^{1/3} Ai'[0]}{Pr^{1/3} Ai[0](ik|k| - (ik)^{2/3} Ai'[0])}. \tag{25}$$

Using the Fourier inversion theorem, we can obtain the pressure distribution, skin friction, and displacement thickness for any given surface-temperature function. The solutions of the linearized equations are shown in the next section compared with the nonlinear solutions.

4. Nonlinear Steady Analysis

For values of T_w not close to unity, the complete solution of the problem defined by the steady form of (12)–(16) requires numerical treatment. In terms of the Fourier transformed variables, defined in the previous section, the nondimensional nonlinear equations take the form

$$ik u_F + \frac{dv_F}{d\bar{y}} = 0, \tag{26}$$

$$ik\bar{y}\tau_F - \frac{d^2\tau_F}{d\bar{y}^2} = -\left\{\hat{u}\frac{\partial\hat{\tau}}{\partial\bar{x}}\right\}_F - \left\{\hat{v}\frac{\partial\hat{\tau}}{\partial\bar{y}}\right\}_F - \left\{\frac{d\hat{p}}{d\bar{x}}\frac{d\hat{T}}{\partial\bar{y}}\right\}_F, \tag{27}$$

$$ik\bar{y}T_F - \frac{1}{Pr}\frac{d^2T_F}{d\bar{y}^2} = -\left\{\hat{u}\frac{\partial\hat{T}}{\partial\bar{x}}\right\}_F - \left\{\hat{v}\frac{\partial\hat{T}}{\partial\bar{y}}\right\}_F, \tag{28}$$

$$u_F = \int_0^y \tau_F(s)\,ds \tag{29}$$

$$p_F = |k|\int_0^\infty (\tau_F(\bar{y}) - T_F(\bar{y}))\,d\bar{y}, \tag{30}$$

with the boundary conditions

$$T_F(0) = T_{wF}, \qquad \left.\frac{d\tau_F}{d\bar{y}}\right|_{\bar{y}=0} - p_F = \left\{\hat{T}_w\frac{d\hat{p}}{d\bar{x}}\right\}_F, \qquad \tau_F(\infty)\to 0, \qquad T_F(\infty)\to 0. \tag{31}$$

In the above equations we have eliminated the transformed displacement function A_F and have replaced it by the transformed version of the boundary condition

$$A_F = \int_0^\infty [\tau_F(\bar{y}) - T_F(\bar{y})]\,d\bar{y}.$$

The pressure, p_F, can also be suppressed by introducing (30) into the boundary condition (31).

We use a pseudospectral technique similar to that employed in [22] and [23]. We normalize the transversal coordinate for the lower deck in the following form:

$$\zeta = \frac{\bar{y}}{1+\bar{y}}.$$

The nonlinear terms are placed at the right-hand side of (26) (28). The procedure employed to initiate the calculations is to neglect these nonlinear terms and compute the Fourier transformed variables for the whole domain in k. The nonlinear terms are then included in the next iteration after evaluating the products in physical space, using results of the previous iteration and twice the fast fourier transform routine. We add an artificial transient term in the governing equations and use the "time" increment as a relaxation parameter. This procedure is repeated until convergence is achieved. The convergence criterion involved a tolerance of 10^{-5} in the pressure in the whole domain. Aliasing is removed using the 3/2 rule [24]. We use

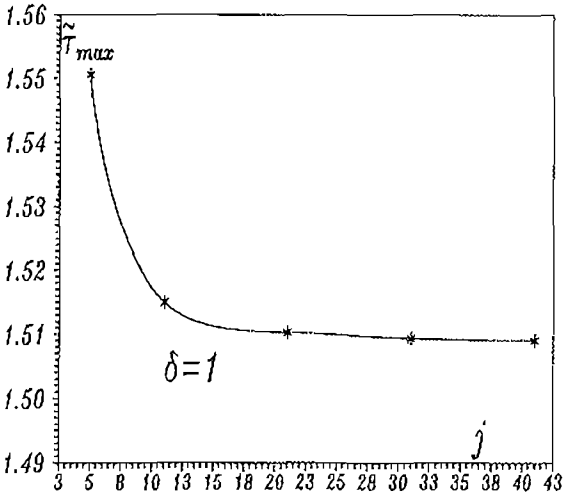

Figure 2. Influence of the number of grid points in the transversal coordinate on the maximum value of skin friction for $\delta = 1$.

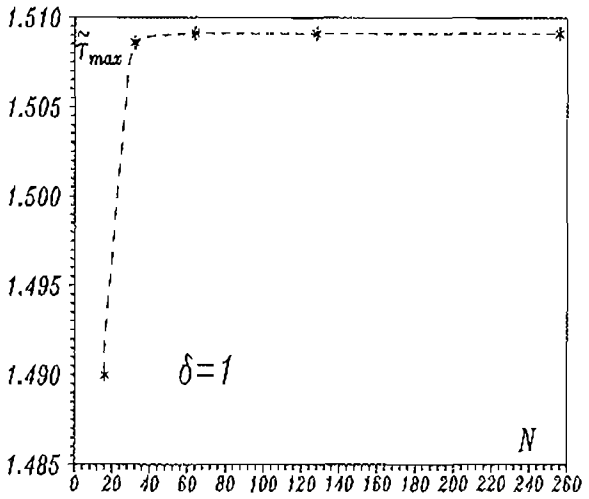

Figure. 3. Influence of the number of modes on the maximum value of skin friction for $\delta = 1$.

finite central differences to evaluate the derivatives in the left-hand side of (26) (31). The first derivative evaluated at the surface for the boundary condition is discretized by second-order accurate backward differences [22]. The integrals in (29) and (30) are approximated using the trapezoidal rule. We assume a heating function of the form

$$\hat{T}_w = \frac{\delta}{1 + \bar{x}^2},$$

with δ now of order unity. The corresponding Fourier transformed variable is then $T_{wF} = \pi\delta \exp(-|k|)$. All numerical computations of the nonlinear governing triple-deck equations have been performed at the Cray-YMP computer of the National University of Mexico. The calculations presented here were made using a grid of $j = 41$ points in the transversal direction and $N = 256$ modes in the longitudinal coordinate, with the following endpoints $x_f = \pm 10\pi$. It gives a resolution in the Fourier space of $\Delta k = 0.2$. This grid size was obtained after analyzing its influence on the resulting profiles using a heating parameter, $\delta = 1$. Figures 2 and 3 show this influence on the maximum value of the wall skin function, $\tilde{\tau}$, $\tilde{\tau}_{max}$. In Figure 2 we vary the number of grid points in the transversal direction but maintain a constant number of modes, $N = 256$. It can be seen that $\tilde{\tau}_{max}$ reaches almost a constant value of 1.5091 for $j > 30$. On the other hand, in Figure 3 we show the influence of the variation in the number of modes on $\tilde{\tau}_{max}$, maintaining a constant number of grid points in the transversal direction, $j = 41$. Sixty four modes are enough to reproduce with high accuracy the value of $\tilde{\tau}_{max} = 1.5091$. Figure 4 shows the nondimensional pressure distribution, $\tilde{p}$, for $\delta = 1$ for both the linearized and the full nonlinear equations, using the 256 modes and a fluid with Prandtl number unity. In fact what is plotted, at least for the linear case, is $\tilde{p}\, Pr^{1/3}/\delta$. Due to the gas expansion, there are two regions with adverse pressure gradients at the edges of the triple-deck middle zone, together with a favorable pressure-gradient region around the maximum plate temperature. The pressure first increases due to the expansion effects in the lower deck. Downstream the pressure decreases strongly reaching values lower than the ambient pressure, increasing again slowly asymptotically to the ambient value, for large positive values of $\bar{x}$. These adverse pressure gradients have a big influence in regions close to the wall, where the convective terms are small. The nonlinear effects are rather small upstream of the maximum temperature point. However, there are two main effects due to the nonlinearities downstream. The peak of the minimum pressure is shifted further downstream and the underpressure itself is reduced. Figure 5 shows the nondimensional shear stress at the wall. For relatively large negative values of $\bar{x}$, the adverse pressure gradient produces a decreasing shear stress at the wall. The second adverse pressure-gradient region (for positive values of $\bar{x}$) also produces a peak (stronger than the upstream one) in the minimum shear stress at the wall. The peak in the nondimensional wall shear stress, produced by the favorable pressure gradient close to $\bar{x} = 0$, is much more pronounced than the two peaks in both adverse pressure regions. Thus, it is

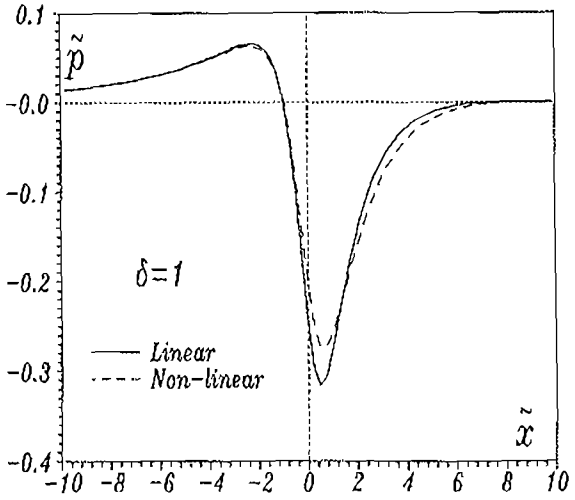

Figure 4. Nondimensional pressure distribution induced by a wall-temperature law given by $T_w^* = T_\infty^*[1 + 1/(1 + x^{*2})]$.

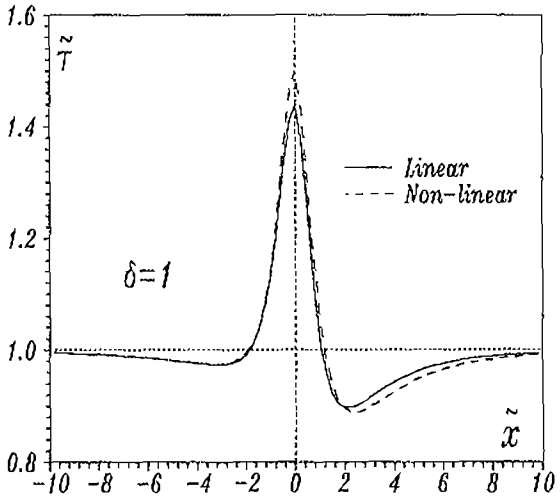

Figure 5. Nondimensional skin-friction distribution induced by a wall-temperature law given by $T_w^* = T_\infty^*[1 + 1/(1 + x^{*2})]$.

shown that cooling (instead of heating) will reduce the minimum wall shear stress for similar temperature differences. The critical conditions for separation can be obtained ($\tilde{\tau} = 0$) from the linear analysis, giving the extremely large value of $\delta_{cl} \approx 10\, Pr^{1/3}$. Practically, it is not possible to obtain separation using this smooth heating form. Figure 6 shows the values of the minimum values of the wall shear stress as a function of nondimensional temperature ratio δ, for both the linear and nonlinear analyses. Surprisingly, there is not a big influence of the nonlinearities on that value, for values of $\delta \leqslant 4$. For values of δ smaller than 3, the nonlinear effects tend to decrease this minimum wall shear stress. However, for larger values of δ, the effect of the nonlinearities tries to reduce this value compared with the linear analysis. Therefore, separation will occur at larger values of δ as predicted by linear extrapolation. Figure 7 shows the maximum value of the wall shear stress as a function of δ. The nonlinear effects always tend to increase this value.

The nondimensional pressure distribution and skin friction or wall shear stress for the cooling process are plotted in Figures 8 and 9, respectively, for the minimum possible value of the parameter δ, $\delta = -1$. For the linear case, the results are exactly the same, but with the sign changed, indicating the existence of a region with a strong adverse pressure gradient surrounded by two regions with moderately favorable pressure gradients. In this case a high-pressure zone develops in the central region producing a strong

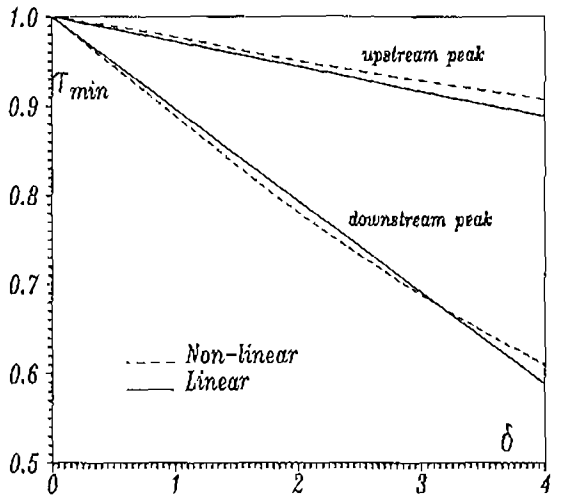

Figure 6. Minimum skin-friction values as a function of the nondimensional temperature ratio δ.

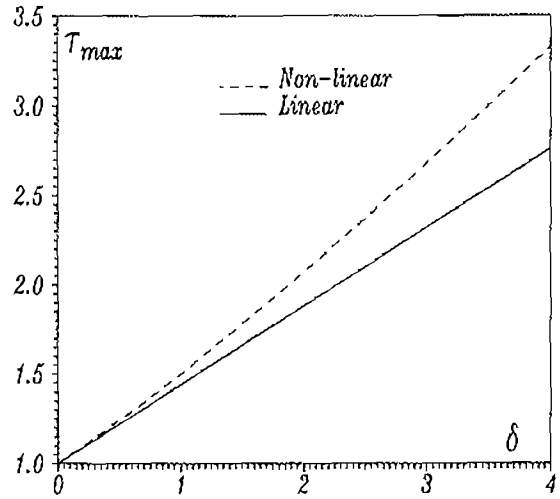

Figure 7. Maximum skin-friction values as a function of the nondimensional temperature ratio δ.

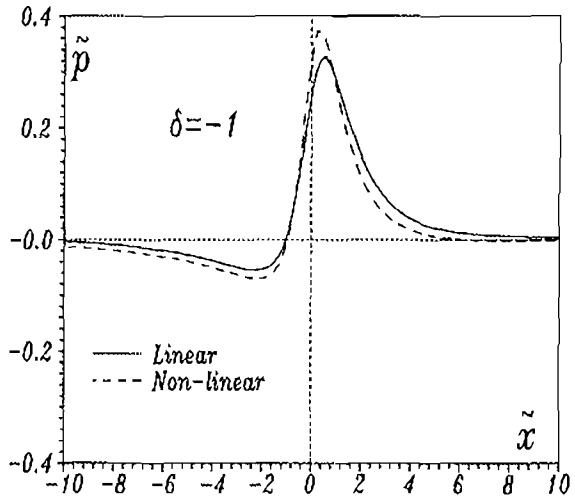

Figure 8. Nondimensional pressure distribution induced by a wall-temperature law given by $T_w^* = T_\infty^*[1 - 1/(1 + x^{*2})]$.

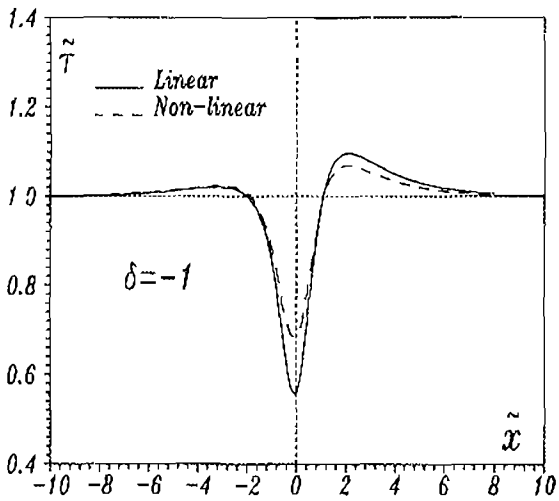

Figure 9. Nondimensional skin-friction distribution induced by a wall-temperature law given by $T_w^* = T_\infty^*[1 - 1/(1 + x^{*2})]$.

reduction in the minimum wall shear stress as indicated in those figures. However, separation cannot be achieved with the cooling process. Here, again, the nonlinear terms try to increase the minimum value of the wall shear stress.

Figures 10 and 11 show the nondimensional pressure distribution and wall shear stress for different positive (heating) values of δ. Increasing the temperature ratio, both peaks, the minimum pressure and the minimum wall shear stress, are shifted downstream. We got convergence problems as we increased the value of δ further. We could not obtain a steady-state solution for values of $\delta > 4$, with the required convergence tolerance.

5. Stability Analysis

In this section we analyze the effect of a space-periodic surface thermal perturbation on lower branch boundary-layer stability, for high Reynolds numbers. To study this effect on boundary-layer stability, we assume a small monochromatic thermal perturbation, of order δ, with a given wave number β. In this case

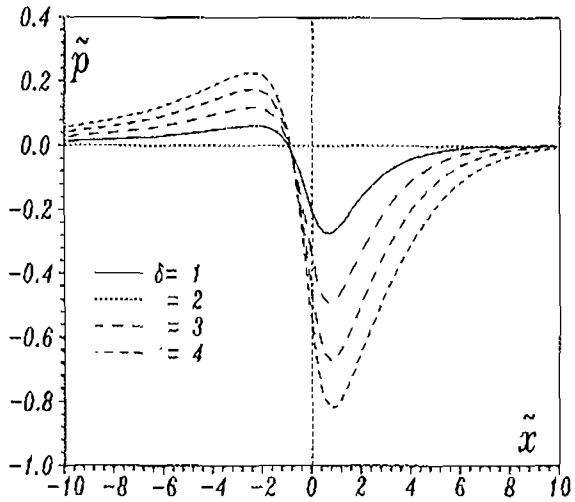

Figure 10. Nondimensional pressure distribution induced by a wall-temperature law given by $T_w^* = T_\infty^*[1 + 1/(1 + x^{*2})]$ for different values of δ.

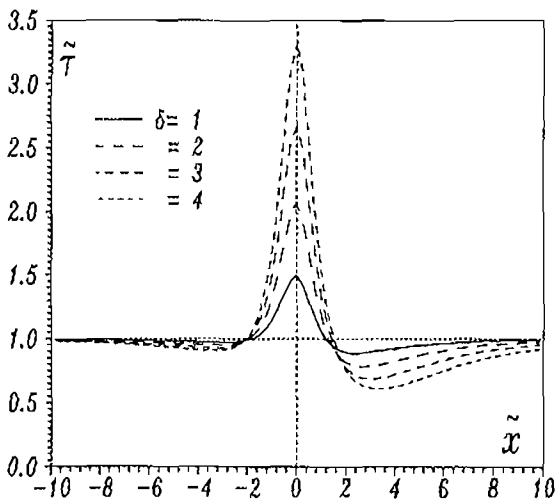

Figure 11. Nondimensional skin-friction distribution induced by a wall-temperature law given by $T_w^* = T_\infty^*[1 + 1/(1 + x^{*2})]$ for different values of δ.

we assume a solution of the form

$$\hat{\tau} = \sum_{n=0}^{\infty} \delta^{n+1} \hat{\tau}_n(\bar{x}, \bar{y}) + \varepsilon \sum_{n=0}^{\infty} \delta^n \hat{\varphi}_n(\bar{x}, \bar{y}, \bar{t}), \tag{32}$$

$$\hat{T} = \sum_{n=0}^{\infty} \delta^{n+1} \hat{T}_n(\bar{x}, \bar{y}) + \varepsilon \sum_{n=0}^{\infty} \delta^n \hat{\theta}_n(\bar{x}, \bar{y}, \bar{t}), \tag{33}$$

$$\hat{p} = \sum_{n=0}^{\infty} \delta^{n+1} \hat{p}_n(\bar{x}, \bar{y}) + \varepsilon \sum_{n=0}^{\infty} \delta^n \hat{\Pi}_n(\bar{x}, \bar{y}, \bar{t}), \tag{34}$$

where $\delta \to 0$ and $\varepsilon/\delta \to 0$. Introducing these relationships into the triple-deck governing equations, we obtain, after collecting terms of the order ε,

$$\frac{\partial \hat{\varphi}_0}{\partial \bar{t}} + \bar{y} \frac{\partial \hat{\varphi}_0}{\partial \bar{x}} - \frac{\partial^2 \hat{\varphi}_0}{\partial \bar{y}^2} = 0, \tag{35}$$

with the appropriate boundary conditions. We assume $\hat{\varphi}_0$ to be given by

$$\hat{\varphi}_0 = \sum_{k=0}^{\infty} \{F_{0k}(\bar{y}) \exp[i(k\bar{x} - \omega_{0k}\bar{t})] + F_{0k}^*(\bar{y}) \exp[-i(k\bar{x} - \omega_{0k}^*\bar{t})]\}, \tag{36}$$

where F_{0k}^* and ω_{0k}^* denote the complex conjugate of the respective variable. ω_{0k} is the first term of the expansion

$$\omega_k = \sum_{n=0}^{\infty} \delta^n \omega_{nk}.$$

Equation (35) transforms to

$$i(k\bar{y} - \omega_{0k}) F_{0k} = \frac{d^2 F_{0k}}{d\bar{y}^2}, \tag{37}$$

with boundary conditions

$$\left.\frac{dF_{0k}}{d\bar{y}}\right|_{y=0} = ik|k| \int_0^{\infty} F_{0k}\, d\bar{y}, \qquad \lim_{\bar{y} \to \infty} F_{0k} = 0. \tag{38}$$

Equations (37) and (38) represent the perturbation on the incompressible boundary (lower branch), studied deeply by Smith and Burggraf [25], [26]. These equations reduce to the well-known dispersion relation

$$Ai'(\chi) = [ik]^{2/3} |k| \int_{\chi}^{\infty} Ai(s)\, ds \tag{39}$$

with

$$\chi = -\omega_{0k} \frac{(ik)^{1/3}}{k}.$$

However, as mentioned by Smith [26], it is preferable to obtain the solution numerically (iteratively), giving an initial guess of ω_{0k}. This eigenvalue problem can be modified to the following boundary-value problem:

$$i(k\bar{y} - \omega_{0k}) f_{0k} = \frac{d^2 f_{0k}}{d\bar{y}^2}, \tag{40}$$

with the boundary conditions

$$\left.\frac{df_{0k}}{d\bar{y}}\right|_{y=0} = ik|k|, \qquad \lim_{\bar{y} \to \infty} f_{0k} = 0 \tag{41}$$

and the restriction

$$\int_0^{\infty} f_{0k}(\bar{y})\, d\bar{y} = 1. \tag{42}$$

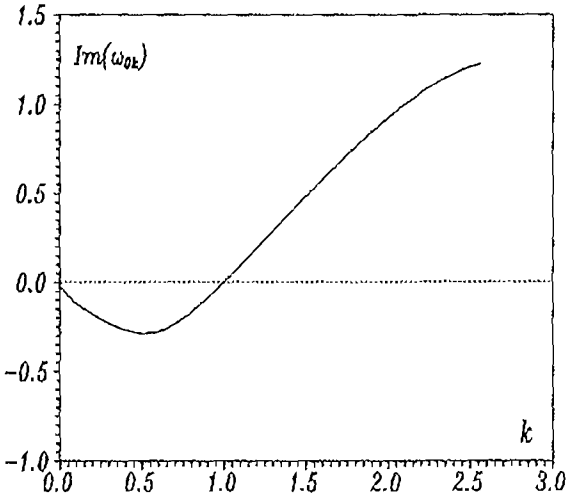

Figure 12. Leading-order value of the nondimensional growth rate $\mathrm{Im}(\omega_{0k})$ as a function of the wave number k.

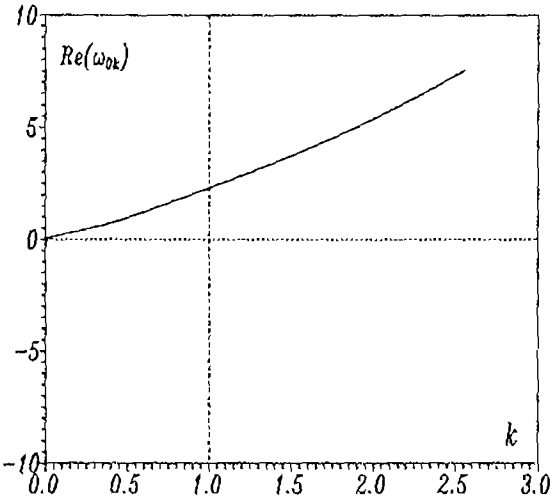

Figure 13. Leading-order value of the nondimensional frequency $\mathrm{Re}(\omega_{0k})$ as a function of the wave number k.

Equations (40) and (41) are numerically integrated giving an initial guess of the eigenvalues ω_{0k}. This value is corrected using the restriction condition (42) by the formula

$$\omega_{0k} = k\left[|k| + \bar{y}_{\infty} - \frac{iv_{0\infty k}}{ku_{0\infty k}}\right], \tag{43}$$

where the velocity components

$$u_{0\infty k} = \int_0^{\bar{y}_{\infty}} F_{0k}(\tilde{y})\,d\tilde{y}, \qquad v_{0\infty k} = -ik\int_0^{\bar{y}_{\infty}} u_{0\infty k}(\bar{y})\,d\bar{y} \tag{44}$$

are obtained in a previous iteration for a large fixed value of $\bar{y}, \bar{y}_{\infty}$. This procedure is continued until convergence is achieved. Figures 12 and 13 show the results for the eigenvalue ω_{0k} as a function of the wave number k. The boundary-layer flow is unstable for positive values of the imaginary part of ω_{0k}. We obtain the well-known values of neutral stability, for $k = k_c = 1.0004\ldots$ with a nondimensional frequency, real part of $\omega_{0k} = 2.297\ldots$. Figure 14 shows the phase shift of both the nondimensional transversal velocity component in the main deck as well as the nondimensional vorticity at the wall, with the resulting pressure distribution, as a function of the wave number k. The nondimensional vorticity in the main deck is also plotted in the same figure. As the value of k reaches the value of k_c, the transversal velocity component

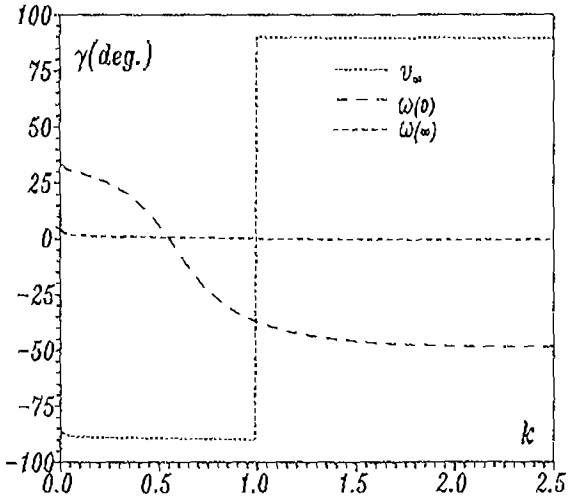

Figure 14. Phase shift between pressure distribution and some flow variables.

changes in sign. In this case, for $k > k_c$, any pressure perturbation generates the conditions in the lower deck that induce a flow in the upper deck tending to increase such a perturbation. In order to study surface thermal effects on boundary-layer stability, we have to go further by collecting terms of order $\varepsilon\delta$, giving

$$\frac{\partial\hat{\phi}_1}{\partial\bar{t}} + \bar{y}\frac{\partial\hat{\phi}_1}{\partial\bar{x}} - \frac{\partial^2\hat{\phi}_1}{\partial\bar{y}^2} = -U_0\frac{\partial\hat{\phi}_0}{\partial\bar{x}} - u_0\frac{\partial\hat{\tau}_0}{\partial\bar{x}} - V_0\frac{\partial\hat{\phi}_0}{\partial\bar{y}} - v_0\frac{\partial\hat{\tau}_0}{\partial\bar{y}} - \frac{\partial\hat{\Pi}_0}{\partial\bar{x}}\frac{\partial\hat{T}_0}{\partial\bar{y}} - \frac{\omega_{1k}}{\omega_{0k}}\frac{\partial\hat{\phi}_0}{\partial\bar{t}}, \tag{45}$$

where

$$U_0 = \int_0^\infty \hat{\tau}_0\, d\bar{y}, \qquad V_0 = -\int_0^\infty \frac{\partial U_0}{\partial\bar{x}}\, d\bar{y}, \qquad u_0 = \int_0^\infty \hat{\phi}_0\, d\bar{y}, \qquad v_0 = -\int_0^\infty \frac{\partial u_0}{\partial\bar{x}}\, d\bar{y}. \tag{46}$$

In Fourier transform space, (45) takes the form

$$\begin{aligned} i(k\bar{y} - \omega_{0k})F_{1k} - \frac{d^2F_{1k}}{d\bar{y}^2} = {} & i\omega_{1k}F_{0k} - i[U_{0\beta}F_{0(k-\beta)}(k-\beta) + U^*_{0\beta}F_{0(k+\beta)}(k+\beta)] \\ & - i\beta[u_{0(k-\beta)}\hat{\tau}_{0\beta} + u_{0(k+\beta)}\hat{\tau}^*_{0\beta}] - \left[V_{0\beta}\frac{dF_{0(k-\beta)}}{d\bar{y}} + V^*_{0\beta}\frac{dF_{0(k+\beta)}}{d\bar{y}}\right] \\ & - \left[v_{0(k-\beta)}\frac{d\hat{\tau}_{0\beta}}{d\bar{y}} + v_{0(k+\beta)}\frac{d\hat{\tau}^*_{0\beta}}{d\bar{y}}\right] - i\left[\Pi_{0(k-\beta)}(k-\beta)\frac{d\hat{T}_{0\beta}}{d\bar{y}} + \Pi_{0(k+\beta)}(k+\beta)\frac{d\hat{T}^*_{0\beta}}{d\bar{y}}\right]. \end{aligned} \tag{47}$$

The monochromatic temperature perturbation can be written as

$$T_w = \frac{\delta}{2}\{\exp[i(\beta\bar{x} + \alpha)] - \exp[-i(\beta\bar{x} + \alpha)]\}, \tag{48}$$

where α is the phase shift. Up to first order in δ, the solution in Fourier space is given by

$$\hat{T}_{0\beta} = \frac{\exp(i\alpha)Ai[(i\beta Pr)^{1/3}\bar{y}]}{2Ai[0]}, \tag{49}$$

$$\hat{\tau}_{0\beta} = \frac{\exp(i\alpha)i\beta|\beta|Ai[(i\beta)^{1/3}\bar{y}]}{2Pr^{1/3}Ai[0](i\beta|\beta| - (i\beta)^{2/3}Ai'[0])}, \tag{50}$$

$$\hat{p}_{0\beta} = \frac{\exp(i\alpha)|\beta|(i\beta)^{1/3}Ai'[0]}{2Pr^{1/3}Ai[0](i\beta|\beta| - (i\beta)^{2/3}Ai'[0])}. \tag{51}$$

In (49)–(51) addition of the complex conjugate is implied. The solvability condition gives the first-order correction for the complex frequency perturbation, ω_{1k}, which measures the effect of surface thermal perturbation on boundary-layer stability. This value can be found after solving the adjoint problem defined by

$$-i(k\bar{y} - \omega^*_{0k})G_k - \frac{d^2G_k}{d\bar{y}^2} = ik|k|G_k(0), \tag{52}$$

with boundary conditions

$$\left.\frac{dG_k}{d\bar{y}}\right|_{\bar{y}=0} = 0, \qquad \lim_{\bar{y}\to\infty} G_k(\bar{y}) = 0.$$

In fact, the asymptotic behavior for large values of $\bar{y}$ is given by

$$\frac{G_k}{G_k(0)} \sim -\frac{|k|}{(\bar{y} - \omega^*_{0k}/k)} + \frac{2|k|}{k(\bar{y} - \omega^*_{0k}/k)^4} + \cdots. \tag{53}$$

Figures 15–17 show the first-order correction for the growth rate, $\mathrm{Im}(\omega_{1k})$, for all leading-order stable wave numbers k ($k < k_c$) and different values of the thermal perturbation wave number β. All possible phase shifts

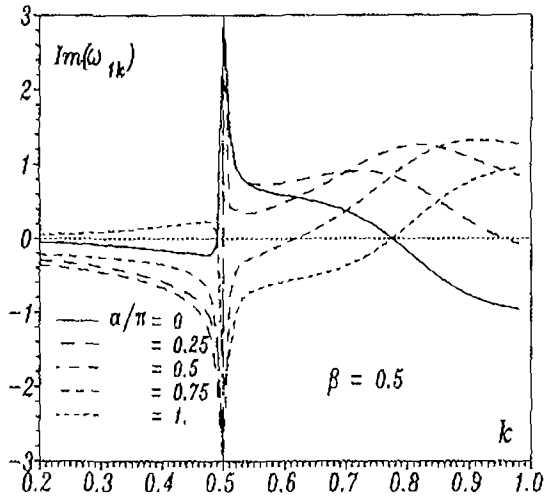

Figure 15. First-order value of the nondimensional growth rate as a function of the wave number k for $\beta = 0.5$.

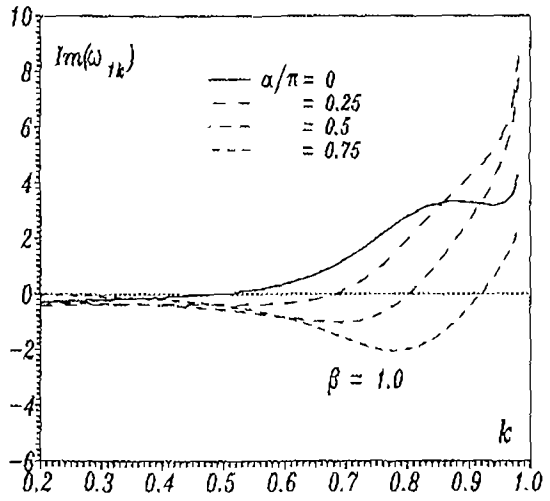

Figure 16. First-order value of the nondimensional growth rate as a function of the wave number k for $\beta = 1$.

are scanned in the upper half-plane $0 < \alpha < \pi$. The corresponding phase shifts to the lower half-plane can be obtained using the fact that $\mathrm{Im}[\omega_{1k}(\alpha)] = -\mathrm{Im}[\omega_{1k}(-\alpha)]$. Due to this, the important variable is the absolute value of the first-order correction of the eigenvalue, ω_{1k}. In all three figures we can see how monochromatic thermal perturbation, with amplitude δ, modifies boundary-layer neutral stability, causing all wave numbers to be unstable, depending on the value of δ. The same results are shown in Figures 18 and 19 for ω_{1k} as a function of the wave number of the thermal perturbation β, for a given fixed value of k. The shift of the neutral stability curve, which depends not only on the parameter δ, but also on the perturbation wave number β, can be obtained up to first order from the relationship

$$\mathrm{Im}[\omega_{0k}] + \delta_{ck}\{\max(\mathrm{Im}[\omega_{1k}(\alpha, \beta)]\} = 0, \tag{54}$$

where $\delta_{ck}(\beta)$ corresponds to the temperature ratio which makes any perturbation of wave number k unstable. The biggest influence occurs for $k = \beta$, resulting in a resonant-type interaction which produces the singularity in the figures. Figure 20 shows δ_{ck} as a function of k for different values of the thermal

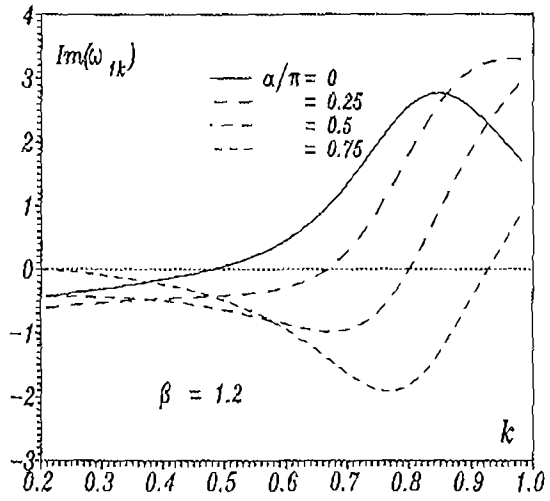

Figure 17. First-order value of the nondimensional growth rate as a function of the wave number k for $\beta = 1.2$.

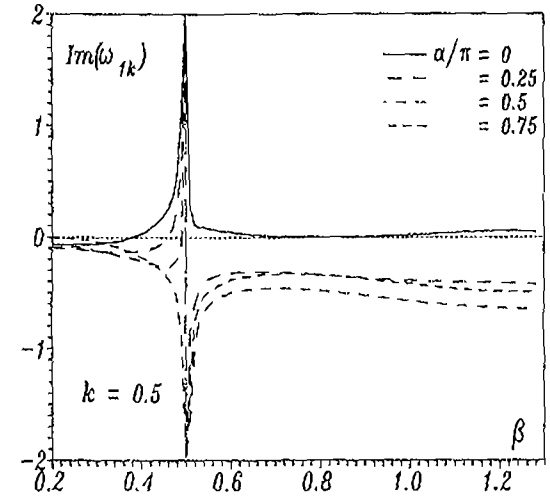

Figure 18. First-order value of the nondimensional growth rate as a function of the perturbation wave number β for $k = 0.5$.

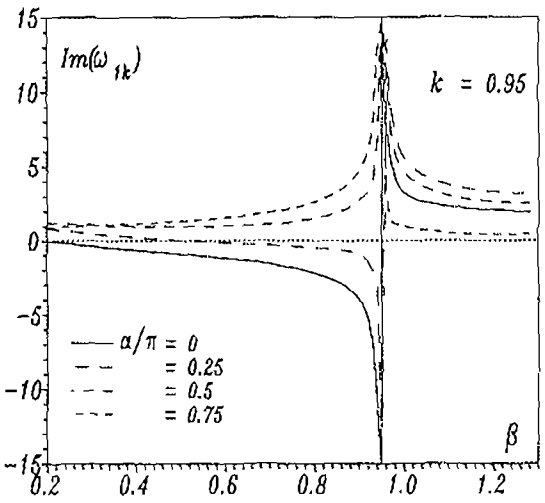

Figure 19. First-order value of the nondimensional growth rate as a function of the perturbation wave number β for $k = 0.95$.

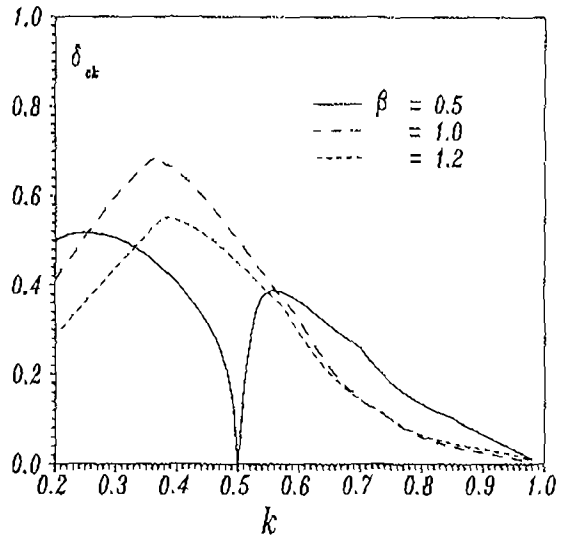

Figure 20. Critical value of the thermal surface intensity δ as a function of the wavenumber k for different values of β.

perturbation wave number β. Relatively small values of δ are needed to make, up to first order, the boundary-layer flow unstable for all wave numbers.

6. Concluding Remarks

The structure and stability of a gaseous boundary-layer flow perturbed by thermal effects at the body surface, was analyzed in this work using the formalism of triple-deck theory. The nonconstant density unsteady governing equations are reduced to the quasi-incompressible case by using the Howarth–Dorodnitzyn transformation for an ideal gas with the Chapman–Rubesin parameter of unity. The linear and nonlinear steady triple-deck governing equations have been numerically integrated using spectral numerical methods. Both heating and cooling were analyzed using a smooth surface-temperature distribution given by $T_w^* = T_\infty^*[1 + \delta/(1 + x^{*2})]$. For the values of the heating parameter δ considered, $-1 < \delta < 4$, it was not possible to obtain boundary-layer separation for the smooth surface-temperature profile assumed. For larger values of δ it was not possible to obtain a steady-state solution with the appropriate convergence tolerance. The heating profile studied in Fourier space is $\pi\delta \exp(-|\bar{x}|)$, which clearly contains unstable modes. Using linear analysis, the critical conditions for boundary-layer separation give the extremely large value of $\delta_{cr} = 10\, Pr^{1/3}$. Practically, it is impossible to get boundary-layer separation using this smooth profile, contrary to that obtained using a step change in surface temperature [6]. For the same values of $|\delta|$, cooling reduces in a stronger way the minimum wall shear stress, but without any possibility of separation. Using perturbation methods, we have obtained first-order correction of the lower branch neutral stability curve for the boundary-layer flow. This correction is produced by a low-intensity monochromatic surface thermal perturbation, in a gaseous flow. The shift of the neutral stability is then computed for different values of the thermal perturbation wave number β. We obtained both quantitatively and qualitatively the effect of wall thermal perturbation on the stability of the boundary-layer flow, making unstable some otherwise stable modes, depending on the temperature ratio.

References

[1] K. Stewartson and P.G. Williams, Self-induced separation, *Proc. Roy. Soc. London Ser. A*, vol. 312, pp. 181–206 (1969).

[2] A.F. Messiter, Boundary layer flow near the trailing edge of a flat plate, *SIAM J. Appl. Math.*, vol. 18, pp. 241–257 (1970).

[3] K. Stewartson, D'Almbert's paradox, *SIAM Rev.*, vol. 23, pp. 308–343 (1981).

[4] F.T. Smith, On the high Reynolds number theory of laminar flows, *J. Appl. Math.*, vol. 28, pp. 207–281 (1982).

A.F. Messiter and A. Liñán, The vertical flat plate in laminar free convection: effects of leading and trailing edges and discontinuous temperature, *Z. Angew. Math. Phys.*, vol. 27, pp. 633–651 (1976).
F. Méndez, C. Treviño, and A. Liñán, Boundary layer separation by a step in surface temperature, *Internat. J. Heat Mass Transf.*, vol. 35, pp. 2725–2738 (1992).
F.T. Smith, On the non-parallel flow stability of the Blasius boundary layer, *Proc. Roy. Soc. London Ser. A*, vol. 366, pp. 91–109 (1979).
F.T. Smith, Non-linear stability of boundary layers for disturbances of various sizes, *Proc. Roy. Soc. London Ser. A*, vol. 368, pp. 573–589 (1979).
F.T. Smith, *Proc. Roy. Soc. London Ser. A*, vol. 371, p. 439 (1980).
M.E. Goldstein, Scattering of acoustic waves into Tollmien-Schlichting waves by small streamwise variations in surface geometry, *J. Fluid Mech.*, vol. 154, p. 509 (1985).
M.E. Goldstein and L.S. Hultgren, A note on the generation of Tollmein-Schlichting waves by sudden surface-curvature change, *J. Fluid Mech.*, vol. 181, p. 519 (1987).
P. Leehey and P. Shapiro, Leading edge effect in laminar boundary layer excitation by sound, in *Laminar-Turbulent Transition* (ed. R. Eppler and H. Fasel), Springer-Verlag, New York, pp. 321–331 (1979).
R.J. Bodonyi, W.J.C. Welch, P.W. Duck, and M. Tadjfar, A numerical study of the interaction between unsteady free-stream disturbances and localized variations in surface geometry, *J. Fluid Mech.*, vol. 209, p. 285 (1989).
S.O. Seedougui, R.I. Bowles, and F.T. Smith, Surface-cooling effects on compressible boundary-layer instability, and on upstream influence, *European J. Mech. B/Fluids*, vol. 10, p. 117 (1991).
V.I. Lysenko and A.A. Maslov, The effect of cooling on supersonic boundary-layer stability, *J. Fluid Mech.*, vol. 147, p. 39 (1984).
S.N. Brown, H.K. Cheng, and C.J. Lee, Inviscid–viscous interaction on triple-deck scales in a hypersonic flow with strong wall cooling, *J. Fluid Mech.*, vol. 220, p. 309 (1990).
D.L. Turcotte, Stable combustion of a high velocity gas in a heated boundary layer, *J. Aeronaut. Sci.*, vol. 27, pp. 509–516 (1960).
T. Hirano and Y. Kanno, Aerodynamical and thermal structures of a laminar boundary layer over a flat plate with a diffusion flame, *Proc. XIV Internat. Symp. on Combustion*, p. 391 (1973).
C. Treviño, W. Stüttgen, and N. Peters, Pressure gradients due to gas expansion and gasification effects in a boundary layer combustion of a condensed fuel, *Wärme Stoffübertrag.*, vol. 25, pp. 309–319, (1990).
C. Treviño, W. Stüttgen, and N. Peters, Higher order effects in the premixed boundary layer combustion, *J. Propul. Power*, vol. 6, no. 3, pp. 237–242 (1990).
L. Howarth, Concerning the effect of compressibility on laminar boundary layers and their separation, *Proc. Roy. Soc. London Ser. A*, vol. 194, p. 16 (1948).
P.W. Duck and O.R. Burggraf, Spectral solutions for three-dimensional triple-deck flow over surface topography, *J. Fluid Mech.*, vol. 162, pp. 1–22 (1986).
O.R. Burggraf and P.W. Duck, Spectral computation of triple-deck flows, in *Numerical and Physical Aspects of Aerodynamic Flows* (ed. T. Cebeci), Springer-Verlag, New York (1981).
C. Canuto, M.Y. Hussaini, A. Quarteroni and T.A. Zang, *Spectral Methods in Fluid Dynamics*, Springer-Verlag, New York (1988).
F.T. Smith and O.R. Burggraf, On the development of large-sized short scaled disturbances in boundary layers, *J. Proc. Roy. Soc. London Ser. A*, vol. 399, p. 25 (1985).
F.T. Smith, On the first mode instability in subsonic, supersonic or hypersonic boundary layers, *J. Fluid Mech.*, vol. 198, pp. 127–153 (1989).